Effect of OH Internal Torsion on the OH-Stretching Spectrum of *cis,cis*-HOONO

Daniel P. Schofield and Henrik G. Kjaergaard*

Department of Chemistry, University of Otago, P.O. Box 56, Dunedin, New Zealand

Received: November 7, 2004; In Final Form: December 15, 2004

We show that a simple two-dimensional vibrational model can explain most of the features observed in the first and second OH-stretching overtone region of the room temperature *cis,cis*-HOONO spectrum. The model uses ab initio calculated parameters and includes the OH-stretching mode coupled to the internal torsion of the OH group.

Introduction

The three-body reaction

$$OH + NO_2 + M \rightarrow HONO_2 + M \qquad (1)$$

is important in atmospheric chemistry as it is a sink for the reactive HO_x and NO_x families. The implications of nitric acid deposition make this reaction important, particularly in polluted atmospheres where the concentration of NO_2 is high.[1] It has been suggested that under atmospheric conditions there may be a secondary reaction in which OH and NO_2 combine to form a small amount of peroxynitrous acid (HOONO).[2] Recently, Golden and co-workers used a master equation approach to predict an upper limit of around 20% formation of HOONO due to the interaction of OH and NO_2 near the tropopause.[3]

Spectroscopic verification of this secondary channel was first provided by Nizkorodov and Wennberg, who recorded the vibrational overtone photodissociation spectrum (so-called action spectrum) of HOONO in the first OH-stretching overtone region.[4] The spectrum of HOONO has since been recorded in the fundamental OH-stretching region using cavity ringdown spectroscopy,[5] and in the first[6−8] and second[7] OH-stretching overtone regions using action spectroscopy.

Assignment of the rich vibrational structure present in the action spectra of HOONO has proved difficult. It has been proposed that the spectra are complicated by the presence of structural conformers of HOONO.[4,7,8] The conformers are named according to the conformation about the ONOO and NOOH dihedral angles, respectively. The most stable conformer of HOONO is the planar *cis,cis* conformer shown in Figure 1.[5,9]

The spectrum recorded by Nizkorodov and Wennberg in the first OH-stretching overtone region consisted of at least seven partially overlapping bands and most of these bands were tentatively assigned to the different conformers of HOONO.[4] The intensity distribution in the spectrum was at odds with the estimated populations of each of the conformers as the strongest peak was assigned to the energetically unfavored *trans-perp* conformer.[4] This conformer is calculated with the CCSD(T)/cc-pVTZ method to be 3.4 kcal/mol higher in energy than the *cis,cis* conformer[5] and thus at room temperature should have a minimal contribution to the vibrational spectrum. Based on their experiments, Fry et al. have recently suggested that all peaks observable in their room-temperature spectrum of HOONO are due to the *cis,cis* conformer.[8]

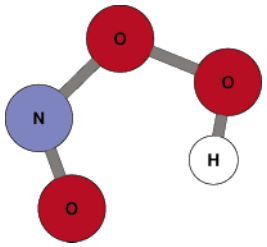

Figure 1. The QCISD/6-311++G(2d,2p) optimized structure of HOONO.

The local mode theory of vibration[10−12] has been used extensively to model highly vibrationally excited XH-stretching modes where X = C, N, or O.[12] However, attempts to simulate the OH-stretching peak positions in HOONO using a one-dimensional OH-stretching anharmonic local mode model have not been able to reproduce the rich vibrational structure that is observed.[7,8] In this work, we simulate the spectrum of *cis,cis*-HOONO in the OH-stretching regions using a local mode Hamiltonian that includes the OH-stretching mode coupled to the NOOH-torsional mode of vibration. The approach we use is similar to that used successfully to describe CH-stretching overtone spectra of methyl groups affected by internal rotation.[13−16]

The main aim of this paper is to show that a simple two-dimensional vibrational model, with no adjustable parameters, can explain most of the complex structure observed in the OH-stretching overtone spectrum of HOONO.

Theory and Computational Methods

The oscillator strength of a transition from a vibrational ground state g to a vibrationally excited state e is given by[17]

$$f_{eg} = 4.702 \times 10^{-7}[\text{cm D}^{-2}]\tilde{\nu}_{eg}|\vec{\mu}_{eg}|^2 \qquad (2)$$

where $\tilde{\nu}_{eg}$ is the transition frequency in wavenumbers, and $\vec{\mu}_{eg} = \langle e|\vec{\mu}|g\rangle$ is the transition dipole moment in Debye.

Vibrational Hamiltonian. Our vibrational Hamiltonian includes the OH-stretching mode coupled to the NOOH-torsional mode. The torsional mode is expressed by the torsional angle θ, and the OH-stretching mode by the internal displacement coordinate q. The angular dependence of the torsional potential V_{tor}, and of the OH-stretching frequency $\tilde{\omega}$ and anharmonicity

* To whom correspondence should be addressed. E-mail: henrik@alkali.otago.ac.nz. Fax: 64-3-479-7906. Phone: 64-3-479-5378.

10.1021/jp0448999 CCC: $30.25 © 2005 American Chemical Society
Published on Web 02/15/2005

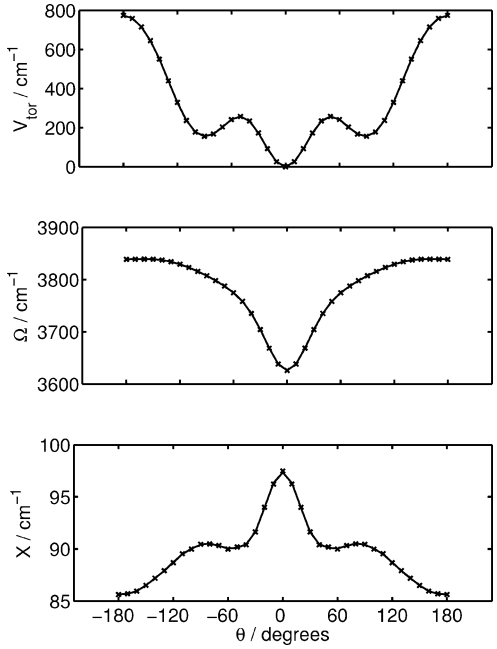

Figure 2. The torsional potential (V_{tor}), frequency (Ω), and anharmonicity (X) as a function of the torsional angle. Both the QCISD/6-311++G(2d,2p) calculated values ($\times$) and the 12th order Fourier fit (solid line) are shown.

$\tilde{\omega}x$ are fitted with Fourier series. We follow the notation of Rong and Kjaergaard[13] and write the approximate stretch-torsion Hamiltonian as

$$\hat{H} = Bm^2 + V_{tor}(\theta)F + \left(v + \frac{1}{2}\right)\Omega(\theta)F - \left(v + \frac{1}{2}\right)^2 X(\theta)F \quad (3)$$

where B is the rotational constant, v and m are the number of quanta in the stretching and torsional modes, respectively, and the Fourier series terms are expressed by a column vector $F = [1, \cos(\theta), \cdots, \cos(12\theta), \sin(\theta), \cdots, \sin(12\theta)]^T$. We assume that B remains constant with vibrational excitation. V_{tor}, Ω, and X are the vectors containing the respective Fourier series expansion coefficients.

The expansion coefficient vectors are obtained from a series of ab initio calculations. The molecule is optimized for different values of the torsional angle θ from 0° (*cis,cis* conformer) to 180° (*cis,trans* conformer) in 10° steps. The energies obtained from these calculations provide $V_{tor}(\theta)$ and are shown in Figure 2. The OH-stretching frequency and anharmonicity at each torsional angle are obtained from the 2nd (f_{ii}), 3rd (f_{iii}), and 4th (f_{iv}) order derivatives of the potential energy with respect to the OH-stretching coordinate according to[18,19]

$$\tilde{\omega} = \frac{\sqrt{f_{ii}G_{ii}}}{2\pi c} \quad (4)$$

$$\tilde{\omega}x = \frac{\hbar G_{ii}}{2\pi c f_{ii}}\left(\frac{5f_{iii}^{\ 2}}{48f_{ii}} - \frac{f_{iv}}{16}\right) \quad (5)$$

where G_{ii} is the reciprocal of the OH reduced mass. Previously we have obtained $\tilde{\omega}x$ by using the expression derived by Sowa et al.,[21] which depends only on the 2nd- and 3rd-order derivatives of the energy.[20] We have recently found that use of eq 5 gives $\tilde{\omega}x$ values that are in better agreement with experimental observations for H_2O.[18]

We determine the force constants by fitting an 8th order polynomial to an ab initio calculated nine point grid. The grid is obtained by calculating the energy at values of q ranging from −0.2 to 0.2 Å in steps of 0.05 Å. We repeat the process in 10° steps of θ from 0° to 180°. In Figure 2 we show the calculated variation in $\tilde{\omega}$ and $\tilde{\omega}x$ with torsional angle as well as the Fourier series fit to these points. We fit the calculated V_{tor}, $\tilde{\omega}$, and $\tilde{\omega}x$ in a least-squares sense with a Fourier series truncated at 12th order. The Fourier coefficients up to 6th order are given in Table 1 with the full set of coefficients given in the Supporting Information. The decreasing values of the coefficients indicates that the series converge with increasing order. There are no sin($m\theta$) terms in the expansions due to the symmetry of the system.

TABLE 1: The Coefficients (in cm^{-1}) of the Fourier Series Expansion of the Potential (V_{tor}), Frequency (Ω), and Anharmonicity (X)

	QCISD/6-311++G(2d,2p)			QCISD/6-31+G(d,p)		
	V_{tor}	Ω	X	V_{tor}	Ω	X
1	321.6	3781.4	89.8	198.0	3764.8	89.6
cosθ	−279.9	−83.5	3.7	−168.8	−86.2	3.6
cos(2θ)	118.3	−35.2	0.2	93.7	−32.7	0.4
cos(3θ)	−99.4	−17.2	1.5	−88.0	−15.8	1.5
cos(4θ)	−51.2	−11.1	1.0	−24.6	−10.9	1.2
cos(5θ)	−7.3	−4.8	0.5	−5.3	−4.9	0.6
cos(6θ)	−2.7	−2.3	0.3	−6.4	−2.1	0.3

We have used the product of a Morse oscillator function with a real rigid rotor function as our vibrational basis functions. The rigid rotor basis functions are cos($m\theta$) and sin($m\theta$), where m is the torsional quantum number. We have limited m to 12, and therefore have 25 torsional states associated with each vibrational level. We obtain our vibration-torsion eigenfunctions and eigenenergies by diagonalizing our Hamiltonian in this basis. We have found that a basis with $m \leq 12$ was sufficient to ensure a converged solution in agreement with previous work on methyl torsion.[13]

Dipole Moment Function. The dipole moment function necessary for the calculation of intensities is expressed in terms of q and θ. The dipole moment is a vector and all three components have to be considered. The expansion of the x-component can be written in matrix form as[13]

$$\mu_x = QC_xF \quad (6)$$

where $Q = [1, q, q^2, ..., q^6]$. The matrix C_x contains the dipole moment expansion coefficients and is determined in a manner similar to the V_{tor}, Ω, and X vectors. For each of the torsional angles from 0° to 180° a 15 point grid of dipole moments was calculated at values of the OH-stretching coordinate ranging from −0.3 to 0.4 Å in steps of 0.05 Å. The dipole moment values of the 15 point grids are then fitted with 6th order polynomials to obtain the coefficients with respect to q for the different values of θ. The angular dependence of these coefficients was subsequently found by fitting them to a 12th order Fourier series. We required a larger grid size for the calculation of our dipole moment coefficient matrix than for the V_{tor}, Ω, and X vectors due to slower convergence of the higher order dipole moment expansion terms in q. The y- and z-components of the dipole are determined in a similar manner. The dipole moment expansion coefficient matrixes C_x, C_y, and C_z are given as Supporting Information.

All grid points and geometry optimizations were calculated with the QCISD level of theory and the 6-31+G(d,p) and 6-311++G(2d,2p) basis sets within the Gaussian03 program.[22] It has been found that these methods give accurate OH-stretching intensities.[23]

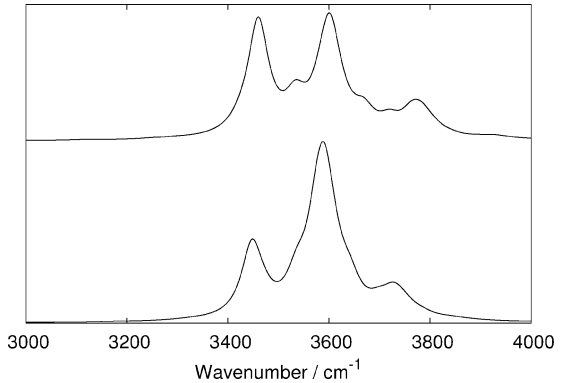

Figure 3. The simulated spectrum of *cis,cis*-HOONO at 298 K in the $\Delta v_{OH} = 1$ region. The bottom trace is calculated with the QCISD/6-31+G(d,p) parameters and the top trace with the QCISD/6-311++G(2d,2p) parameters.

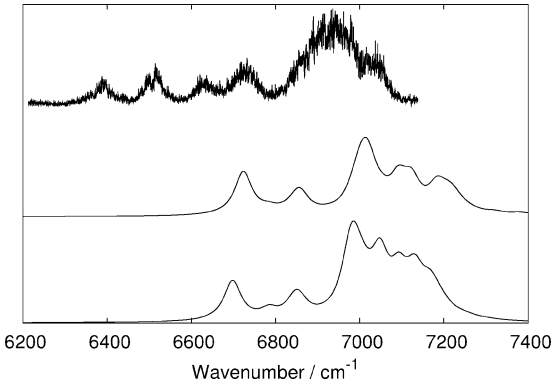

Figure 4. The experimental (top) and QCISD/6-311++G(2d,2p) (middle) and QCISD/6-31+G(d,p) (bottom) simulated spectra of *cis,cis*-HOONO at 298 K in the $\Delta v_{OH} = 2$ region.

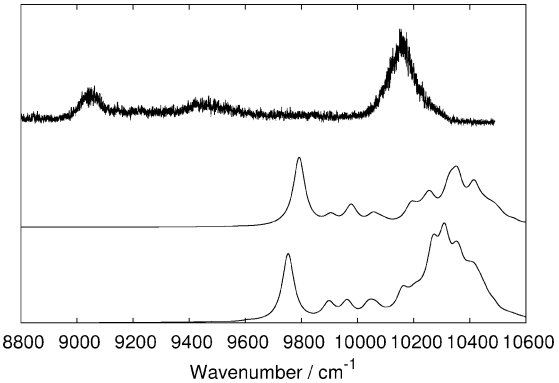

Figure 5. The experimental (top) and QCISD/6-311++G(2d,2p) (middle) and QCISD/6-31+G(d,p) (bottom) simulated spectra of *cis,cis*-HOONO at 298 K in the $\Delta v_{OH} = 3$ region.

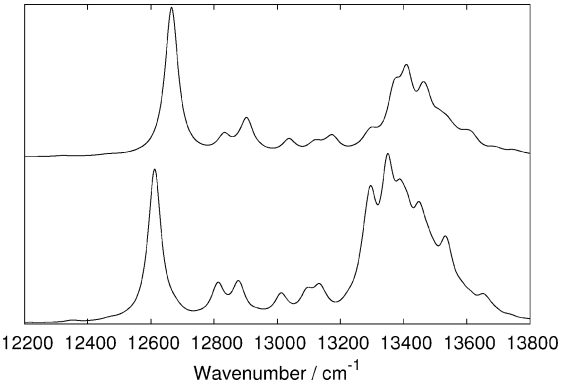

Figure 6. The simulated spectrum of *cis,cis*-HOONO at 298 K in the $\Delta v_{OH} = 4$ region. The bottom trace is calculated with the QCISD/6-31+G(d,p) parameters and the top trace with the QCISD/6-311++G(2d,2p) parameters.

Spectral Simulation. We simulate the HOONO spectrum in the regions corresponding to 1−4 quanta in the OH-stretching vibration ($\Delta v_{OH} = 1-4$). The intensity and frequency of all transitions between eigenstates of eq 3 have been calculated with eq 2 and the dipole moment function described in eq 6. Each OH-stretching region consists of transitions between the various torsional eigenstates. Each torsional eigenstate has significant contributions from several of the torsional basis states and cannot be meaningfully labeled in terms of a single basis state. The thermal populations of the torsional states in the vibrational ground state are determined from a Boltzmann distribution. Each transition is convoluted with a Lorentzian of full-width at half-maximum of 50 cm^{-1}, a typical width for an OH-stretching overtone transition.

Results and Discussion

In Figures 3−6 we show our simulated HOONO spectra in the $\Delta v_{OH} = 1-4$ regions. We have simulated these spectra with use of parameters obtained with both the QCISD/6-31+G(d,p) and the QCISD/6-311++G(2d,2p) ab initio methods and we compare these spectra. We also compare with the previously recorded spectra in the $\Delta v_{OH} = 2$ and 3 regions.[4,7,8]

The simulated spectrum of the fundamental OH-stretching region (Figure 3) shows more structure than the one peak expected from a simple one-dimensional OH-stretching model. This additional structure in the OH-stretching region arises from coupling to the torsional mode. We observe some differences in the intensities of the two simulated spectra but the overall profile is similar. The lowest energy peak in the profile is mainly due to the transition between the respective ground torsional eigenstates. Little intensity is present at lower energies than this peak in the simulated profile.

Comparison of QCISD/6-311++G(2d,2p) calculated values of $\tilde{\omega}$ and $\tilde{\omega}x$ to experimental values and higher level calculations for H_2O suggests that at each torsional angle, our QCISD/6-311++G(2d,2p) calculated $\tilde{\omega}$ is around 60−70 cm^{-1} too high, and $\tilde{\omega}x$ is about 2−3 cm^{-1} too high.[18] A correction for this would shift the entire $\Delta v_{OH} = 1$ band about 60 cm^{-1} to the red.[18] So far only a single peak at 3306 cm^1 has been assigned by Bean et al.[5] to the $\Delta v_{OH} = 1$ transition in HOONO. They assigned the peak based on the successful modeling of the absorption profile with a hybrid of a-type and b-type transitions.[5] This peak could certainly be part of our calculated $\Delta v_{OH} = 1$ profile. The presence of strong bands due to $HONO_2$ and HONO in the experimental spectrum prevents a more detailed comparison of our simulated spectrum to experiment in this region.

We compare our two simulated spectra of the first OH-stretching overtone region with the action spectrum of Matthews et al.[7] in Figure 4. The action spectrum is recorded by scanning across a frequency range and if the incoming light source is resonant with a vibrational frequency, HOONO will undergo unimolecular dissociation. The OH fragments that are formed from this dissociation are then detected by laser induced fluorescence of the $A \leftarrow X$ transition at 308 nm.[4,7,8] The three published action spectra of the $\Delta v_{OH} = 2$ region all show a similar band structure with a dominant broad band around 6930 cm^{-1} and four smaller bands at lower energy. However, the intensities in the observed spectra are not quite the same.[4,7,8] It has been shown than the intensity of the peaks is dependent on the quantum state of the OH photofragment detected, particularly

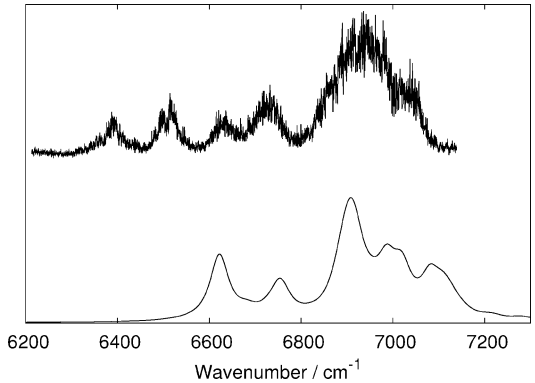

Figure 7. The simulated spectrum of *cis,cis*-HOONO at 298 K in the $\Delta v_{OH} = 2$ region. The bottom trace is calculated with scaled QCISD/6-311++G(2d,2p) parameters and the top trace is the experimental spectrum from ref 7.

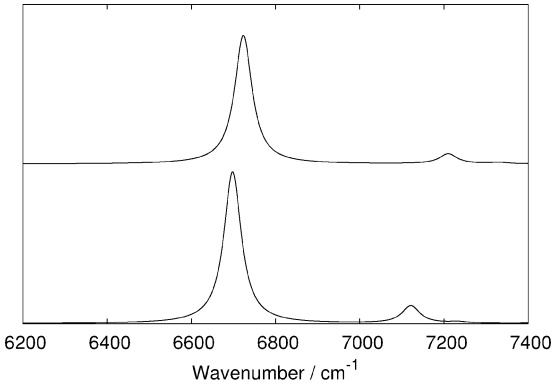

Figure 8. The simulated spectrum of *cis,cis*-HOONO at 5 K in the $\Delta v_{OH} = 2$ region. The bottom trace is calculated with the QCISD/6-31+G(d,p) parameters and the top trace with the QCISD/6-311++G(2d,2p) parameters.

in the $\Delta v_{OH} = 2$ region where the transition energies are close to the dissociation threshold.[7] The observed relative intensities also depend on the quantum yield of dissociation across a particular frequency region. This will be most important near the dissociation threshold, and is difficult to quantify in the experiments performed.

Our two simulated band profiles in the $\Delta v_{OH} = 2$ region show small differences in intensities but the overall band profile is similar. As in the $\Delta v_{OH} = 1$ region, the lowest energy peak in the simulated profile is due to the transition between the ground torsional eigenstates. Substantial intensity is present to the blue of the lowest observed feature. This broad structure arises mainly from transitions between excited torsional eigenstates of the same torsional quantum number. The overall band structure is similar to that observed experimentally; however, the features in the simulated spectra are located at somewhat higher energy. This is expected due to the aforementioned slightly higher local mode parameters calculated with the two QCISD methods used here. The observed dominant structure is centered about 100 cm^{-1} lower than in our simulated spectra, as expected. This structure has contributions from several different transitions similar to what has previously been observed for the CH-stretching overtone spectra of methyl groups involved in internal rotation.[13]

The agreement between experimental and calculated vibrational band positions can be improved by scaling of the OH-stretching local mode parameters, $\tilde{\omega}$ and $\tilde{\omega}x$.[20] To test this we have simulated the spectrum of HOONO with scaled local mode parameters. The scaling factors are obtained from the ratio of observed to QCISD/6-311++G(2d,2p) calculated local mode parameters in hydrogen peroxide (HOOH). The scaling factors are given in the Supporting Information. In Figure 7 we compare our spectrum simulated with scaled local mode parameters to the experimental spectrum in the $\Delta v_{OH} = 2$ region. It can be seen that the positions of the bands in the spectrum simulated using scaled local mode parameters are in much better agreement with the experimental band positions than the simulation shown in Figure 4 using unscaled local mode parameters. Comparison of the two spectra suggests that the two peaks at lowest energy in the experimental spectrum are not reproduced in our simulation. These low energy peaks in the observed spectrum are probably transitions to combination states involving other vibrations such as the OOH-bending mode and/or the OO-stretching mode, which are not included in our model.

The action spectrum of the second OH-stretching overtone region in HOONO has been recorded by Matthews et al.[7] and is compared with our simulated spectra in Figure 5. The spectrum in this region is similar to that in the first overtone region in that the dominant structure is blue-shifted from the transition between the respective torsional ground states calculated to lie around 9790 cm^{-1}. The observed spectrum shows less structure than in the $\Delta v_{OH} = 2$ region. The dominant structure in the observed spectrum at around 10 150 cm^{-1} is about 125 cm^{-1} wide. We suggest that this width is evidence that the structure is composed of several torsional transitions in agreement with our simulations. The observed dominant structure is about 200 cm^{-1} lower in energy than predicted, again in agreement with our estimate of the error in our ab initio calculated local mode parameters.

As in the $\Delta v_{OH} = 2$ spectrum there is a transition observed at lower energy, in this case around 9050 cm^{-1}, which is not in our simulated spectra. This band is probably due to transitions to a state that involve combinations of modes not included in our two-dimensional model.

In Figure 6 we show our two simulated spectra in the $\Delta v_{OH} = 4$ region. The band shapes in the two simulated spectra are again similar and also similar to those in the $\Delta v_{OH} = 2$ and 3 region. It is unfortunate that the spectrum of HOONO in the $\Delta v_{OH} = 4$ region has not yet been recorded. The overall width of the simulated profile increases from the $\Delta v_{OH} = 1$ to the $\Delta v_{OH} = 4$ region. This is similar to what has been observed in the simulation and CH-stretching overtone spectra of internally rotating methyl groups in molecules such as toluene.[24]

We have also performed our simulation at a temperature of 5 K, and the spectrum in the $\Delta v_{OH} = 2$ region is shown in Figure 8. As expected the band structure is much simpler than that seen in the room temperature simulation as only the torsional ground state has appreciable population. We clearly see the dominant transition between torsional ground states around 6700 cm^{-1} as in our room-temperature simulation.

Conclusions

We have used a simple two-dimensional vibrational Hamiltonian to simulate the OH-stretching fundamental and overtone regions of the *cis,cis*-HOONO spectrum. The model includes the OH-stretching vibration coupled to the internal torsion of the OH group. With our simulated spectra of the first and second OH-stretching overtone regions we are able to successfully explain the main features in the recorded action spectra. The richness in the OH-stretching band profile arises from a multitude of transitions between different torsional states. The dominant feature in the previously recorded spectra in the $\Delta v_{OH} = 2$ and 3 regions, as well as our simulated spectra in the Δv_{OH}

= 1−4 regions, lies to the blue of the transition between the respective torsional ground states.

Acknowledgment. We are grateful to Professor Amitabha Sinha and Jamie Matthews for helpful discussions and for supplying us with their spectra. D.P.S is grateful to the Foundation for Research, Science and Technology for a Bright Futures scholarship. We acknowledge computer facilities provided by the Lasers and Applications Research Theme at the University of Otago. The Marsden Fund administered by the Royal Society of New Zealand has provided funding for this research.

Supporting Information Available: One table containing the Fourier series expansion coefficients of the potential, harmonic frequency, and anharmonicity of HOONO; six tables containing dipole moment expansion coefficients of HOONO; and one table containing local mode parameters and scaling factors for HOOH. This material is available free of charge via the Internet at http://pubs.acs.org.

References and Notes

(1) Finlayson-Pitts, B. J.; Pitts, J. N., Jr. *Chemistry of the Upper and Lower Atmosphere*; Academic Press: San Diego, CA, 2000.

(2) Robertshaw, J. S.; Smith, I. W. M. *J. Phys. Chem.* **1982**, *86*, 785−790.

(3) Golden, D. M.; Barker, J. R.; Lohr, L. L. *J. Phys. Chem. A* **2003**, *107*, 11057−11071.

(4) Nizkorodov, S. A.; Wennberg, P. O. *J. Phys. Chem. A* **2002**, *106*, 855−859.

(5) Bean, B. D.; Mollner, A. K.; Nizkorodov, S. A.; Nair, G.; Okumura, M.; Sander, S. P.; Peterson, K. A.; Francisco, J. S. *J. Phys. Chem. A* **2003**, *107*, 6974−6985.

(6) Pollack, I. B.; Konen, I. M.; Li, E. X. J.; Lester, M. I. *J. Chem. Phys.* **2003**, *119*, 9981−9984.

(7) Matthews, J. M.; Sinha, A.; Francisco, J. S. *J. Chem. Phys.* **2004**, *120*, 10543−10553.

(8) Fry, J. L.; Nizkorodov, S. A.; Okumura, M.; Roehl, C. M.; Francisco, J. S.; Wennberg, P. O. *J. Chem. Phys.* **2004**, *121*, 1432−1448.

(9) McGrath, M. P.; Rowland, F. S. *J. Phys. Chem.* **1994**, *98*, 1061−1067.

(10) Henry, B. R. *Acc. Chem. Res.* **1977**, *10*, 207−213.

(11) Henry, B. R. *Acc. Chem. Res.* **1987**, *20*, 429−435.

(12) Henry, B. R.; Kjaergaard, H. G. *Can. J. Chem.* **2002**, *80*, 1635−1642.

(13) Rong, Z.; Kjaergaard, H. G. *J. Phys. Chem. A* **2002**, *106*, 6242−6253.

(14) Rong, Z.; Howard, D. L.; Kjaergaard, H. G. *J. Phys. Chem. A* **2003**, *107*, 4607−4611.

(15) Cavagnat, D.; Lespade, L. *J. Chem. Phys.* **2001**, *114*, 6030−6040.

(16) Zhu, C.; Kjaergaard, H. G.; Henry, B. R. *J. Chem. Phys.* **1997**, *107*, 691−701.

(17) Atkins, P. W.; Friedman, R. S. *Molecular Quantum Mechanics*, 3rd ed.; Oxford University Press: Oxford, UK, 1997.

(18) Kjaergaard, H. G.; Robinson, T. W. Unpublished work.

(19) Herzberg, G. *Molecular Spectra and Molecular Structure I. Spectra of Diatomic Molecules*; D. Van Nostrand Company, Inc.: Princeton, NJ, 1950.

(20) Low, G. R.; Kjaergaard, H. G. *J. Chem. Phys.* **1999**, *110*, 9104−9115.

(21) Sowa, M. G.; Henry, B. R.; Mizugai, Y. *J. Phys. Chem.* **1991**, *95*, 7659−7664.

(22) Frisch, M. J.; Trucks, G. W.; Schlegel, H. B.; Scuseria, G. E.; Robb, M. A.; Cheeseman, J. R.; Montgomery, J. A., Jr.; Vreven, T.; Kudin, K. N.; Burant, J. C.; Millam, J. M.; Iyengar, S. S.; Tomasi, J.; Barone, V.; Mennucci, B.; Cossi, M.; Scalmani, G.; Rega, N.; Petersson, G. A.; Nakatsuji, H.; Hada, M.; Ehara, M.; Toyota, K.; Fukuda, R.; Hasegawa, J.; Ishida, M.; Nakajima, T.; Honda, Y.; Kitao, O.; Nakai, H.; Klene, M.; Li, X.; Knox, J. E.; Hratchian, H. P.; Cross, J. B.; Adamo, C.; Jaramillo, J.; Gomperts, R.; Stratmann, R. E.; Yazyev, O.; Austin, A. J.; Cammi, R.; Pomelli, C.; Ochterski, J. W.; Ayala, P. Y.; Morokuma, K.; Voth, G. A.; Salvador, P.; Dannenberg, J. J.; Zakrzewski, V. G.; Dapprich, S.; Daniels, A. D.; Strain, M. C.; Farkas, O.; Malick, D. K.; Rabuck, A. D.; Raghavachari, K.; Foresman, J. B.; Ortiz, J. V.; Cui, Q.; Baboul, A. G.; Clifford, S.; Cioslowski, J.; Stefanov, B. B.; Liu, G.; Liashenko, A.; Piskorz, P.; Komaromi, I.; Martin, R. L.; Fox, D. J.; Keith, T.; Al-Laham, M. A.; Peng, C. Y.; Nanayakkara, A.; Challacombe, M.; Gill, P. M. W.; Johnson, B.; Chen, W.; Wong, M. W.; Gonzalez, C.; Pople, J. A. *Gaussian 03*, revision c.02; Gaussian Inc.: Wallingford, CT, 2004.

(23) Kjaergaard, H. G.; Henry, B. R. *Mol. Phys.* **1994**, *83*, 1099−1116.

(24) Kjaergaard, H. G.; Rong, Z.; McAlees, A. J.; Howard, D. L.; Henry, B. R. *J. Phys. Chem. A* **2000**, *104*, 6398−6405.